

A MULTIDISCIPLINARY APPROACH TO THE STUDY OF ARCHAEOLOGICAL MORTARS FROM THE TOWN OF AMMAIA IN THE ROMAN PROVINCE OF LUSITANIA (PORTUGAL)*

I. CARDOSO

Universidade de Évora, Laboratório HERCULES, Évora, Portugal

M. F. MACEDO

*Universidade Nova de Lisboa, Faculdade de Ciências e Tecnologia, Departamento de Conservação e Restauro,
VICARTE, Monte da Caparica, Portugal*

F. VERMEULEN and C. CORSI

*Universidade de Évora, CIDEHUS—Centro Interdisciplinar de História, Culturas e Sociedades da Universidade de Évora,
Évora, Portugal*

A. SANTOS SILVA

Laboratório Nacional de Engenharia Civil, Departamento de Materiais, Lisboa, Portugal

L. ROSADO and A. CANDEIAS

HERCULES Lab and Centro de Química de Évora, Évora, Portugal

and J. MIRAÓ†

HERCULES Lab and Centro de Geofísica de Évora, Évora, Portugal

The Roman town of Ammaia (in Marvão Region) is considered one of the most important recent findings of the Roman presence in Portuguese territory. It was settled in Republican times and abandoned in the seventh century. In this research, 17 masonry mortars and renders from the West Tower (South Gate), the residential area near the West Tower, the macellum, the peristylum, the public bath building, the podium of the temple and the portico of the forum were analysed. The methodology of chemical, mineralogical and microstructural characterization has involved several complementary techniques, including stereomicroscopy, X-ray diffraction, thermal analysis and scanning electron microscopy coupled with energy-dispersive X-ray spectroscopy. The results indicate that the mortars from the beginning of the town's edification were mainly composed of soil (clays). Later, during the main Roman building period, mortars were composed using a calcitic binder and the mortar composition varied according to their use and function. The samples from a period subsequent to the Roman occupation are based on a dolomitic binder. From the present study, relevant information has been acquired about the technological evolution of Roman construction in Ammaia, the historical context of the archaeological structures and guidelines for the conservation and restoration of mortars.

KEYWORDS: AMMAIA, ROMAN MORTAR, LUSITANIA, CONSERVATION, XRD, TGA, SEM-EDS

*Received 15 November 2011; accepted 14 December 2012

†Corresponding author: email jmirao@uevora.pt

© University of Oxford, 2013

INTRODUCTION

Ammaia is a Roman town (Fig. 1)—located in present-day Marvão (Portalegre, south-east Portugal)—that was established in the first century BC, at its prime as a prosperous town of Lusitania between the second half of the first century and the end of the second century AD (Vermeulen and Taelman 2010). In the integrated study of *Ammaia*, one of the main tasks was the



Figure 1 An overview of the different structures present in the Roman town of Ammaia: (a) the South Gate (West Tower); (b) the monumental paved square; (c) the macellum; (d) the peristylum; (e) the public bath building; (f) the public bath building (natatio/tepidarium?); (g) the forum—the temple (podium); (h) the forum—the porticus.

study of archaeological mortars, a topic that has received remarkable attention in recent years from many professionals involved in safeguarding Portuguese architectural heritage (Ricardo *et al.* 2005; Silva *et al.* 2006a,b; Velosa *et al.* 2007; Borsoi *et al.* 2010). The case of *Ammaia* shows particular archaeological interest because this town was abandoned and did not suffer subsequent occupation, unlike other cities of Lusitania that were rebuilt in later periods. The study of historical mortars may reveal the knowledge and evolution of construction technologies of a society, as well as its relationship with their surroundings, but also can help in the definition of chronologies and in the detection of the occurrence of ancient reconstructions.

Moreover, the poor state of conservation of the mortars, which consequently affects the archaeological structures, proved to be another concern in this study. Structural fractures, the overthrow of stone blocks and non-functional joints (because they are open, without any filling materials, or the mortars have lost cohesion) are the main deterioration patterns (ICOMOS–ISCS 2008). In many cases, the occurrence of landslides and falling blocks contribute to the structural instability of the archaeological remains. On the other hand, the proliferation of biological colonization/vegetation contributes to the increased fragility of the structures, allowing rainwater infiltration/circulation inside them. Consequently, the binders are continuously lixiviating and alteration of the stones/mortars minerals occurs, which contributes to the loss of cohesion and to disintegration. In addition to these processes, human activity has also become a significant degradation factor, with negative and irreversible consequences.

The chemical, mineralogical and microstructural characterization of 17 masonry mortars and renders was made using complementary techniques such as stereomicroscopy, determination of the soluble fraction:insoluble residue ratio, X-ray diffraction (XRD), thermogravimetric analysis (TGA) and differential thermal analysis (DTA) and scanning electron microscopy coupled with an energy-dispersive X-ray spectroscopy (SEM–EDS). The aims of this research are the determination of the mortar composition (binders, aggregates and additives), their proportions and the raw materials used in their preparation, as well as the production techniques of the mortars. In this sense, the possible occurrence of variations in the composition of the mortars was explored according to their function in the architectural structure and to the social importance of the building. In addition, this study also aimed to support the archaeology team in the definition of different construction periods of the structures. The deterioration patterns of the mortars were also considered and the results of this study were used by the conservators–restorers in the selection and preparation of the restoration mortars, thus ensuring compatibility between them and the pre-existing ones (Delgado Rodrigues and Grossi 2007).

MATERIALS AND METHODS

Sampling

Seventeen samples were collected from archaeological buildings (masonry mortars and renders), using a hammer and a small chisel. The archaeological structures, their historical context, the function of the mortar in the structure, the colour and other details of the samples are shown in Table 1.

Instrumental methods

A photographic record of all of the samples was made (using a Canon PowerShot SX100 IS camera), in addition to observation by the naked eye and through a stereozoom microscope (Leica

Table 1 The identification of the mortar samples from the Roman town of Ammaia

Sample	Location (building function)	Historical context (probably)	Mortar function in the structure/construction technique	Colour	Other relevant characteristics
AM23	South Gate; wall of the West Tower (public)	Islamic or early Middle Ages (reconstruction or eventual restoration?)	<i>Opus mixtum</i> ; masonry mortar	Very pale brown	Small white lumps (lime) Large brown lumps Compact; medium strength
AM24	South Gate; wall of the eventual housing under the paved area (near the West Tower) (private)	Roman (initial period—late first century BC)	Masonry mortar	Strong brown	Grey/dark brown aggregates, in reduced amounts Flat and round morphology Very low degree of cohesion
AM25	<i>Macellum</i> ; exterior wall (public/may have been private at a later stage)	Roman (Islamic?)	<i>Opus caementicium</i> ; masonry mortar	Pale brown	Punctual white lumps (lime) and disaggregated from the other constituents Rather compact (weak link between binder/aggregate) and resistant White lumps (lime) Very compact; medium strength
AM26	<i>Macellum</i> ; interior wall (the same wall, AM25) (public/may have been private at a later stage)	Roman (Islamic?)	<i>Opus caementicium</i> ; masonry mortar	Very pale brown	White lumps (lime) Very compact; medium strength
AM27	<i>Peristylum</i> ; column of the corner of the building (capital of the top) (public)	Islamic or 17th century	Render of a solid brick masonry	Very pale brown	White lumps (lime) Compact; medium strength
AM28	Public bath building, internal wall of the tank (<i>tepidarium</i> or <i>nataatio</i> ?) (public)	Roman	<i>Opus signinum</i> ; <i>opus incertum</i> render for the settlement of the marble slabs (decorative)	Reddish yellow	Reddish fragments, with different hues and dimensions White lumps (lime) Compact; medium strength White lumps (lime)? Compact
AM29	Public bath building; exterior wall of the tank (<i>tepidarium</i> or <i>nataatio</i> ?) (public)	Roman	<i>Opus caementicium</i> ; masonry mortar— <i>opus incertum</i>	Very pale brown	Very high strength (the mortar with the highest strength)
AM30	Public bath building; interior wall of a compartment of the building (public)	Roman	<i>Opus caementicium</i> ; masonry mortar	Very pale brown	White lumps (lime)? Compact; medium strength (Yellow aggregates)
AM31A	Public bath building— <i>porticus</i> ; base of the column (public)	Roman	<i>Opus caementicium</i> ; masonry mortar	Pale brown	Reddish fragments (residual) Compact; high strength

AM3 1B	Public bath building; wall of the <i>porticus</i> (public)	Roman	<i>Opus caementitium</i> ; masonry mortar	Very pale brown	Reddish fragments (residual) Compact; high strength (Yellow aggregates)
AM9B	<i>Forum</i> —temple; filling of the <i>podium</i> of the temple, front face (public)	Roman (end of the first century)	<i>Opus caementitium</i> ; masonry mortar	Very pale brown	Compact; medium strength
AM32	<i>Forum</i> —temple; filling of the <i>podium</i> of the temple, front face, lateral (public)	Roman	<i>Opus caementitium</i> ; masonry mortar	Very pale brown	Compact; medium strength
AM33	<i>Forum</i> —temple; the <i>podium</i> of the temple, traces of inside floor of the <i>cella</i> (public)	Roman	<i>Opus signinum</i> ; render (preparatory layer) for the settlement of the pavement	Light brown (reddish)	Reddish fragments, with different hues and dimensions Compact; medium strength
AM34 (1)*	<i>Forum</i> —temple; the <i>podium</i> of the temple, block of the floor (out of context), that served as filler (reuse) (public)	Roman	<i>Opus signinum</i> ; render (preparatory layer) for the settlement of the pavement	(a) Reddish yellow	Reddish fragments, very coarse, with different hues (three different hues were identified: orange, light red, dark red); other fragments with medium and fine grain size White lumps (lime)? Compact; medium strength
AM35	<i>Forum</i> ; wall of the <i>Porticus</i> , top of the lateral wall (<i>cryptoporticus</i>) (public)	Roman	<i>Opus caementitium</i> ; masonry mortar	(b) Light reddish brown	Reddish fragments with fine grain size White lumps (lime)? Compact; high strength
AM36	<i>Forum</i> — <i>porticus</i> ; reinforcement wall of the <i>cryptoporticus</i> (top), near AM35 (public)	Roman (structure after AM35)	<i>Opus caementitium</i> ; masonry mortar	Very pale brown	Reddish fragments with fine grain size (residual) Large amount of binder Compact; medium strength (Yellow aggregates) Reddish fragments with coarse grain size (residual) Compact; medium strength

*AM34 is a sample composed of two different mortars, which were analysed separately. For this reason, the authors refer to '(a)' and '(b)'.

M205C, with a Leica DFC290HD camera). The samples were cleaned using brushes and a scalpel to remove external materials (e.g., remains of soil and biological colonization) and were disaggregated using a rubber hammer. The global and fine fractions were obtained by passing samples through a 125 μm sieve. Their colours were analysed with reference to the *Munsell Soil Color Chart* (1992) (dry state). After stereomicroscope observations confirming the absence of carbonated aggregates, the disaggregated samples were attacked with warm diluted hydrochloric acid (HCl) (1:3) to separate the soluble fraction (carbonate binder, salts and organic compounds) from the insoluble residue (non-carbonated aggregates). The insoluble residue was sieved for grain size analysis and observed by stereozoom microscope.

The mineralogical characterization of the global fraction was based on XRD, using a Bruker-AXS D8 Advance (Bruker AXS Inc., Madison, WI, USA) diffractometer, with $\text{Cu-K}\alpha$ radiation ($\lambda = 0.15406$ nm), operating at 40 kV and 30 mA. Powder diffraction data were collected in the range $3\text{--}75^\circ$ (2θ) in steps of 0.05° and with a 2 s measuring time per step. The global fraction of the representative samples was also used for thermal analysis (TGA/DTA), performed in a SETARAM TG-DTA instrument, under inert atmosphere (argon, 3 litres h^{-1}) with a uniform heating rate of $10^\circ\text{C min}^{-1}$, from room temperature to 1000°C . The polished surfaces were prepared by vacuum impregnation with epoxy resin, and were observed with the Leica M205C stereozoom microscope, with the Leica DFC290HD camera for image acquisition. The polished surfaces of those samples with the codes AM23, AM28, AM32 and AM34b were coated with carbon and observed on a Hitachi 3700N scanning electron microscope; the chemical composition was obtained by energy-dispersive X-ray spectrometry, using a Bruker Xflash 5010 SDD spectrometer.

RESULTS AND DISCUSSION

Macroscopic observations

Several samples were collected from different archaeological structures of *Ammaia*, to realize their chemical, mineralogical and microstructural characterization; namely, masonry mortars from the West Tower (South Gate) (AM23), the residential area near this tower (AM24), the *macellum* (AM25 and AM26), the public bath building (AM29, AM30, AM31A and AM31B), the *podium* of the temple (AM9B and AM32) and the portico of the *forum* (AM35 and AM36), as well as renders from the column of the *peristylum* (AM27), the inner wall of the tank (public bath building) (AM28) and the preparation of the temple *podium*'s floor (AM33, AM34a and AM34b) (Table 1). Archaeological and historical data established the context of the collected samples from the first century BC, possibly from the beginning of the foundations of the town (AM24), up to the end of the Roman occupation (late fifth century), with the possibility of some samples from the Islamic period/early Middle Ages (AM23) or corresponding to a possible rehabilitation intervention performed in the 17th century (AM27). These buildings had a public function, except for the residential area and the *macellum*—the latter could have been reused as a private space after the Roman occupation (probably during the Islamic period).

Preliminary observation of the samples and the polished surfaces under the stereozoom microscope showed that the mortars are heterogeneous, composed of light-coloured binders and various types of aggregates with respect to their colour, size and angular morphology. Lime lumps were detected, with a compact appearance, rounded shape and variable size, which may indicate that the process of extinction of lime was not complete; that is, a lack of enough water or insufficient time required for the CaO slacking (Callebaut *et al.* 2001; Veiga *et al.* 2004; Adriano and Silva 2006b).

Apart from these characteristics, crushed ceramic fragments were also detected, with different hues of orange/red and sizes, including aggregates in their constitution (e.g., AM28 and AM34). According to the *Munsell Soil Color Chart* (1992), the colours of the fine fraction of the samples vary between 'very pale brown', 'pale brown' and 'strong brown'. The 'light brown' (AM33), 'light reddish brown' (AM34b) and 'reddish yellow' (AM28 and AM34a) are due to the crushed ceramic fragments, present in these samples, with different orange/red hues and grain sizes. Most of the samples presented a lightening of the hues of the global fractions in relation to the fine fraction; this is probably due to the high ratio of light-coloured aggregates—namely, rock crystal and milky quartz—present in the global fraction.

In general, the different constituents are embedded in the binder matrix. The samples are relatively compact and present a medium mechanical strength to the action of the rubber hammer during the disaggregation, with the exception of AM24, which had broken down to a considerable extent. Samples AM28, AM29 (more resistant), AM31A, AM31B and AM34b showed higher mechanical strength than the others (Table 1).

Determination of the soluble fraction:insoluble residue ratio, granulometric analysis and observation of the soluble residue by stereozoom microscope

Figure 2 shows the ratio between the soluble fraction (representative of the binder content, soluble salts, neoformation products resulting from pozzolanic reactions, organic matter etc.) and the insoluble residue (non-carbonated aggregates) obtained for each sample. The soluble fraction:insoluble residue ratio varies from 1:2 (e.g., AM25, AM26, AM27 and AM28) to 1:6 (AM24). In general, unimodal distribution curves (Fig. 3) were obtained and predominant grain size was between 1.0 and 0.5 mm. The increase of the fraction >4 mm in AM28 and AM34a is due to the presence of crushed ceramic fragments; in samples AM24, AM30 and AM31A it is due to aggregates and in sample AM36 to both crushed ceramic fragments and bigger aggregates.

The high amount of fine fractions (<0.125 mm) in samples AM23, AM24, AM33, AM34b, AM35 and AM36 corresponds to the presence of clay fractions, detected by XRD in AM23, AM24, AM35 and AM36. In samples AM33 and AM34b, similar results were obtained, but this fact is mainly due to the presence of crushed ceramic fragments, with a different grain size, observed by their shape and colour under optical microscopy.

After the attack with HCl, the morphological and mineralogical characterization of the insoluble residue was carried out by observation under the stereozoom microscope. In most of the grain size fractions, the dominant mineral is quartz, in hyaline (transparent) and milky (white). The smoked (grey) and citrus (orange) varieties were also identified. Apart from this mineral, the presence of feldspars, micas (muscovite and biotite) and amphibole fragments, igneous rocks (granitoids) and clastic sedimentary rocks (greywacke) is also constant and, less frequently, metamorphic rocks (probably gneiss, quartzite and mica schist).

The observed minerals can be correlated to the local geology (Fig. 4), being derived from the granitic rocks, quartzite and clay schist of the region. Regarding the morphology of the aggregates, the angular shape is predominant, consistent with the proximity (Schiavon and Mazzocchin 2009) of an original outcrop (or materials that have only been transported over short distances); less frequent are the sub-angular (AM32) and rolled (AM25 and AM31A) forms. In addition, the observation of crushed ceramic fragments is confirmed in samples AM28, AM33, AM34a and AM34b, in all grain size fractions (and, therefore, with different

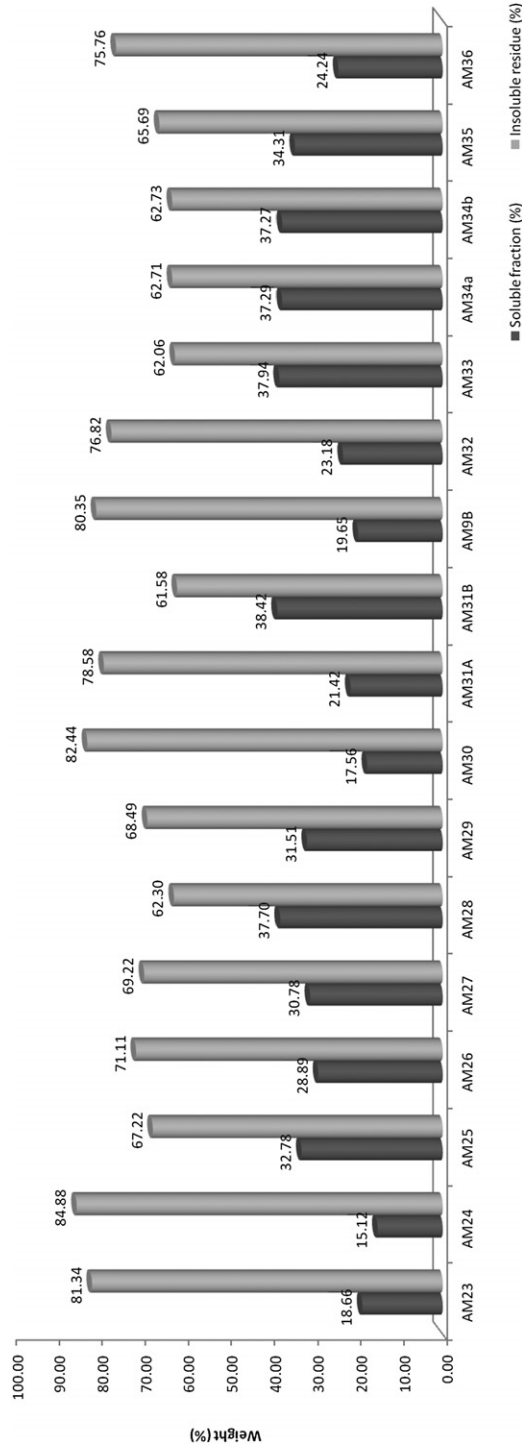


Figure 2 The soluble fraction:insoluble residue ratio.

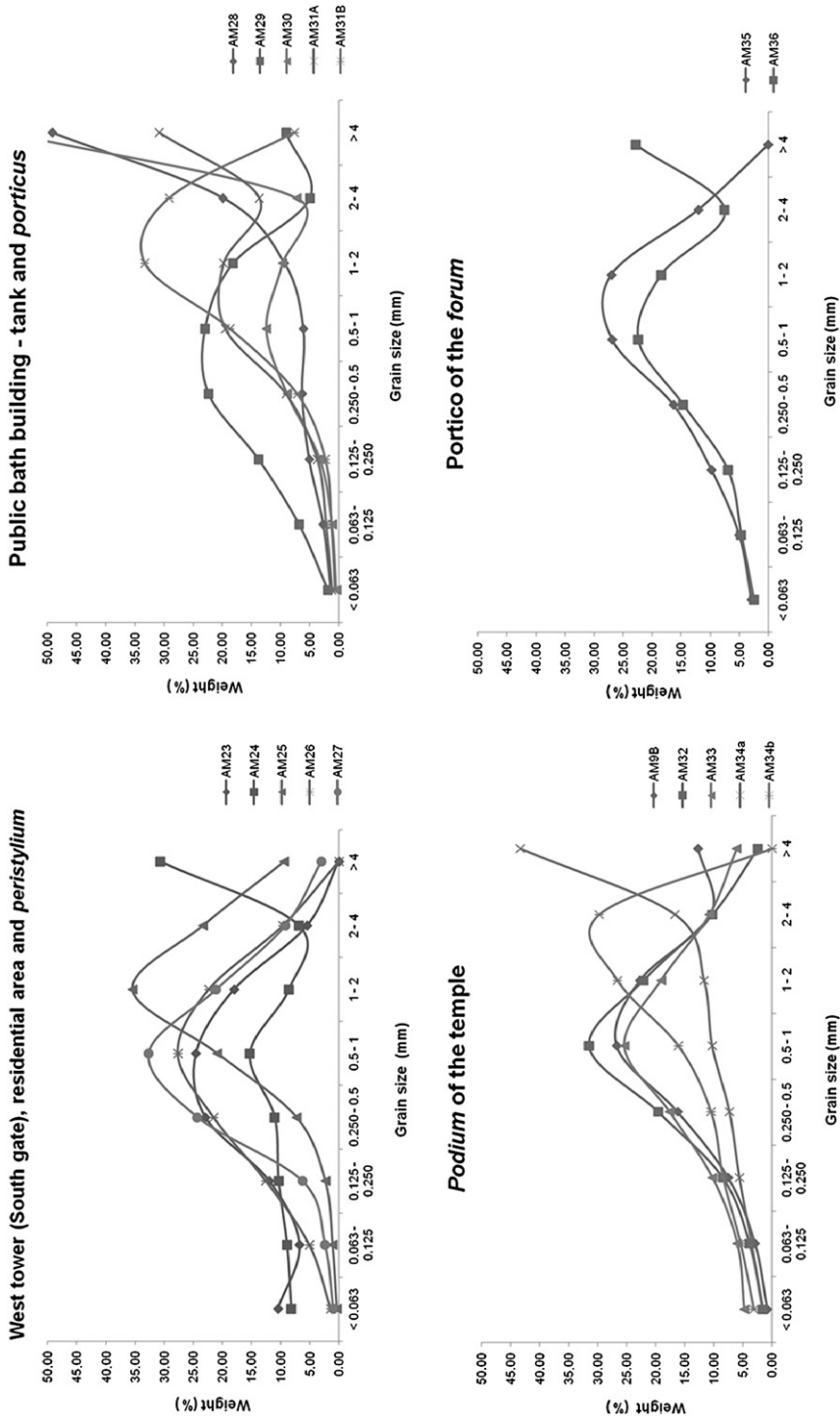


Figure 3 The grain size distribution of the insoluble residues of the analysed mortars (values in %).

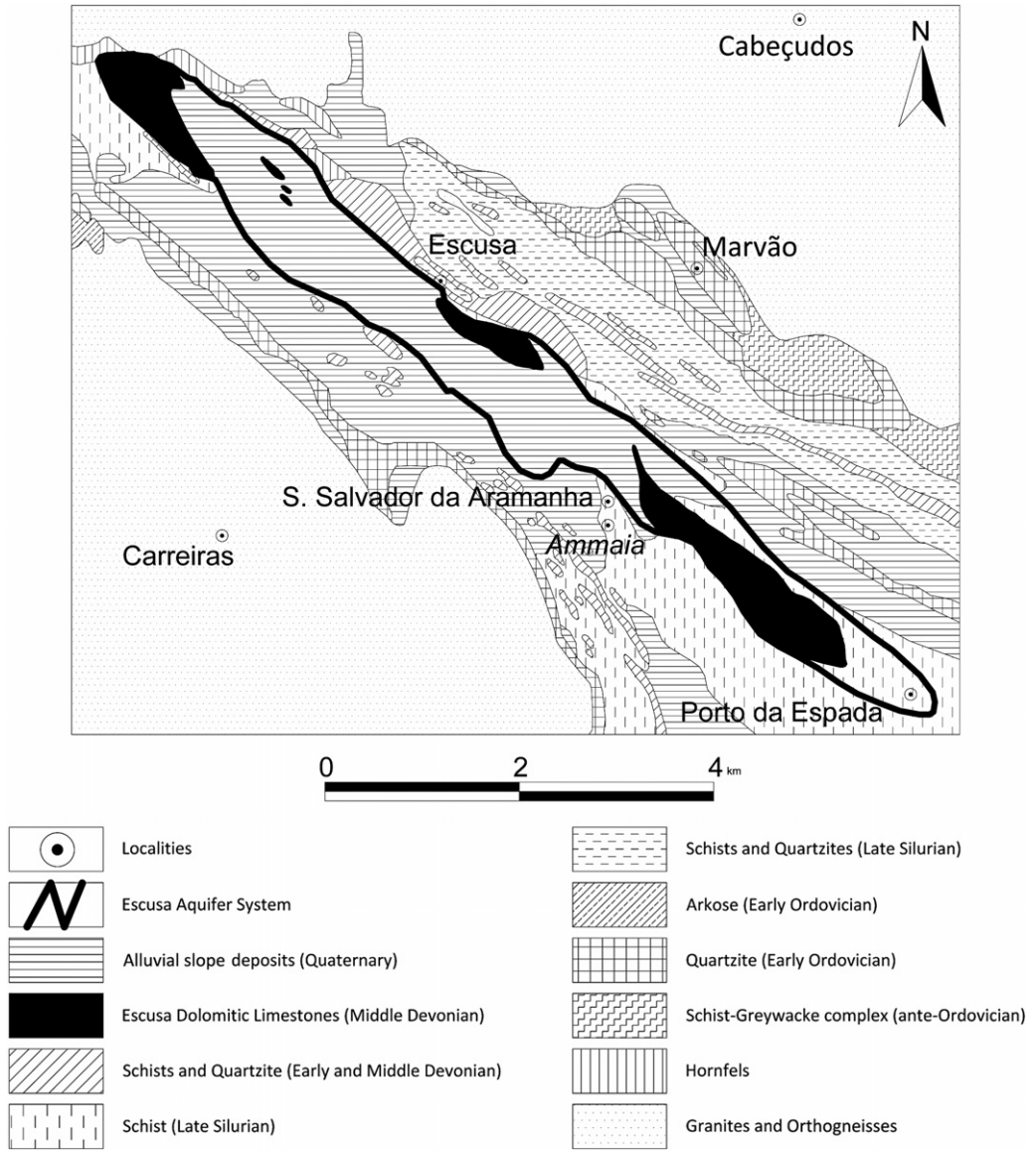


Figure 4 A geological map scheme of the region.

sizes) and different tones of orange/red. The presence of these fragments was also detected in samples AM31A, AM31B, AM35 and AM36, but only in smaller fractions and in residual amounts.

X-ray diffraction

Table 2 presents the qualitative mineralogical composition of the mortars. The XRD results show that the predominant mineral is quartz, which is present in all samples, as well as

Table 2 The mineralogical composition of the mortars (XRD analysis)

Sample	Quartz	Calcite	Feldspars	Illite/mica	Chlorite	Aragonite	Sepiolite	Kaolinite	Amphibole	Cordierite
AM23	+++	+	+++	++	-	-	-	+	-	-
AM24	+++	-	+	+++	+	-	-	-	-	-
AM25	+++	++	+	++	+	-	-	-	-	-
AM26	+++	++	+	+	-	-	-	-	-	-
AM27	+++	++	++	++	+	-	-	-	-	-
AM28	+++	+++	+	+	-	+	-	-	+	-
AM29	+++	++	++	++	-	-	-	-	-	-
AM30	+++	++	++	++	-	-	-	-	-	-
AM31A	+++	+	+	++	+	+	-	-	-	-
AM31B	+++	++	++	+	-	-	-	-	-	-
AM9B	+++	+	++	+	-	-	-	-	-	-
AM32	+++	+	++	+	-	-	-	-	-	-
AM33	+++	++	++	+	+	-	-	-	-	-
AM34a	+++	++	++	+	-	-	-	-	-	+
AM34b	+++	+++	+++	+++	-	-	-	-	-	-
AM35	+++	+++	+++	++	-	-	+	-	-	-
AM36	+++	++	++	+	-	-	+	+	-	-

Peak intensity: ++++, very abundant—predominant compound; +++, abundant; ++, present; +, small amount; -, undetected.

feldspar and mica, although in smaller quantities. Calcite was identified as the main binder, and was more abundant in samples AM25, AM28, AM29, AM30, AM33, AM34b and AM35. The one exception is sample AM24, in which the greatest amount of clay seems to be the main composition of the binder. The detection of aragonite (AM28 and AM31A) may be due to the occurrence of calcite dissolution–recrystallization phenomena (Silva *et al.* 2011). Chlorite, kaolinite, sepiolite, amphibole and cordierite arise in small proportions. The chlorites (a group of phyllosilicates) are constituents of the igneous and metamorphic rocks that were identified during the observation of the aggregates by stereozoom microscope and results from the alteration of biotite, a mineral of the granites that are predominant in the region (Duarte *et al.* 2000). Sepiolite— $\text{Mg}_4\text{Si}_6\text{O}_{15}(\text{OH})_2 \cdot 6\text{H}_2\text{O}$ —is also a clay mineral, the presence of which may be related to the clusters of fine clayish materials in sample AM35, observed by stereozoom microscope. Amphibole is a mineral that occurs in igneous and metamorphic rocks, also identified in sample AM28 during the observation of the aggregates by stereozoom microscope. Cordierite— $(\text{Mg},\text{Fe})_2\text{Al}_3(\text{Si}_5\text{AlO}_{18})$ —is a silicate that occurs associated with feldspar, muscovite and biotite in granitic and schist regions, which relates to the characteristics of the local geology. In general, the results obtained by XRD regarding the abundance of calcite are correlated with the soluble fraction:insoluble residue ratio, obtained by attack with HCl. On the other hand, the observation of the aggregates by stereozoom microscope associated with XRD analysis has shown that their mineralogical composition is related to the local geology (Perdigão and Fernandes 1976). The presence of hydromagnesite ($4\text{MgCO}_3 \cdot \text{Mg}(\text{OH})_2 \cdot 4\text{H}_2\text{O}$), magnesite (MgCO_3) or dolomite ($\text{CaMg}(\text{CO}_3)_2$) was not identified by XRD in any of the samples; these compounds were expected to be indicative of the use of local rocks in the manufacture of lime.

Thermal analysis (TGA/DTA)

Figure 5 presents representative thermograms for the samples analysed by TGA/DTA, while the temperature ranges where significant weight loss occurred are shown in Table 3, as well as the CO_2 /hydraulic water ratio and the hydromagnesite, magnesite and calcite contents. The analysis of the derivative of the TGA and DTA allowed us to determine the following temperature ranges, $<200^\circ\text{C}$, $200\text{--}650^\circ\text{C}$ and $>650^\circ\text{C}$, where significant weight loss occurred.

The weight loss that occurs above 650°C is the decarbonation of CaCO_3 , according to the equation $\text{CaCO}_3 \rightarrow \text{CaO} + \text{CO}_2^\uparrow$ (Moropoulou *et al.* 1995a,b; Bakolas *et al.* 1998; Elsen *et al.* 2010; Silva *et al.* 2011), and it varies between 4.12% (AM23) and 12.51% (AM35) (Table 3), corresponding to 9.37% and 28.38%, respectively, of the CaCO_3 content (see Table 3); these results are corroborated by the soluble fraction:insoluble residue ratio, in which AM23 is richer in insoluble residue and AM35 has an enrichment of the soluble fraction, as seen in Figure 2.

The weight losses that occur at low temperatures ($<120^\circ\text{C}$), and that vary between 0.34% (AM23) and 5.04% (AM28), are due to dehydration of adsorption or hygroscopic water (Moropoulou *et al.* 1995a,b; Bakolas *et al.* 1998; Elsen *et al.* 2010; Silva *et al.* 2011), while in the temperature range from 120°C to 200°C , the weight losses may result in loss of crystallization water of any hydrated salts that are present in the samples (Elsen *et al.* 2010) and physically bound water from silicate constituents of aggregates (Bruni *et al.* 1998). In these ranges, significant weight loss occurs in AM28, AM33, AM34a and AM34b. All these samples have ceramic fragments in their composition and since they are more porous, these materials may favour the retention/presence of physically bound water.

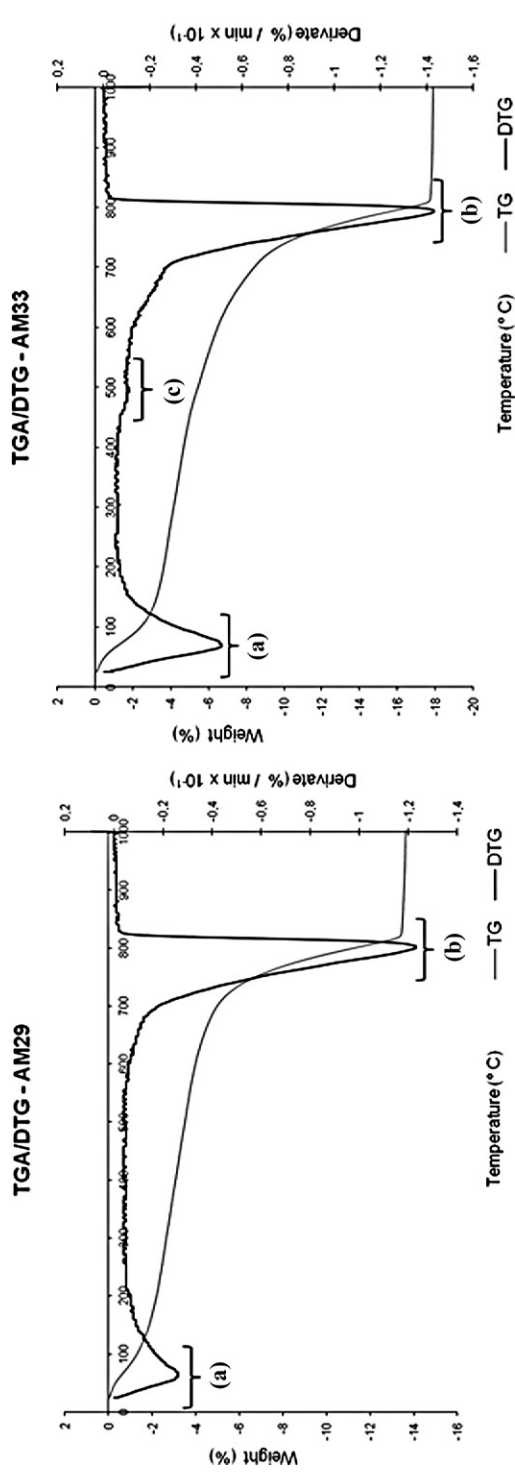


Figure 5 Examples of representative thermograms of the mortar global fractions (AM29 and AM33), in which the significant losses of mass corresponding to (a) water adsorption, (b) calcite decomposition and (c) magnesite decomposition are highlighted.

Table 3 TG/DTA weight losses (%), the CO_2/H_2O ratio, the hydromagnesite, magnesite and calcite contents, and the composition of the mortar samples using the Jedrzejewska method

Samples	Temperature range (°C) and weight loss (%)										Soluble fraction	
	<120	120–200	200–650		>650	CO_2/H_2O^*	HydroMg content†	MgCO ₃ content‡	CaCO ₃ content§	Aggregates¶		
			200–450	450–550						550–650		Siliceous (Si)
AM23	0.34	0.56	0.94	2.08	1.21	4.12	1.92	4.31	3.98	9.37	81.34	5.30
			300→400									
			0.83									
AM26	0.74	0.27	0.88	0.62	0.92	7.36	4.09		1.19	16.74	71.11	10.96
AM27	0.66	0.65	1.38	1.18	1.09	7.35	2.98	5.55	2.26	16.72	69.22	11.81
			300→400									
			1.07									
AM28	5.04	1.82	2.05	0.74	0.77	7.94	2.82		1.42	18.06		18.23
AM29	1.57	0.63		2.17		9.26	4.27			21.06	68.49	10.45
AM30	0.71	0.25		1.45		7.28	5.02			16.56	82.44	1.00
AM9B	1.36	0.50	0.87	0.59	0.83	5.05	2.97		1.13	11.48	80.35	7.04
AM32	1.34	0.55	1.18	0.71	0.79	5.92	3.01		1.36	13.46	76.82	8.35
AM33	2.86	0.74	1.38	0.93	1.35	10.61	3.89		1.78	24.13		12.03
AM34a	3.72	1.49	2.30	0.87	0.93	7.81	2.42		1.67	17.76		17.86
AM34b	1.55	1.33	2.26	0.71	0.83	9.71	3.14		1.36	22.08		13.83
AM35	0.81	0.35	0.76	0.69	0.80	12.51	8.02		1.32	28.45	65.69	4.54
AM36	1.66	0.62	1.12	0.95	1.00	7.03	3.32		1.82	15.99	75.76	6.43

* (Percentage weight loss > 650°C)/(percentage weight loss between 200 and 650°C—excluding the weight losses for the magnesite and hydromagnesite, if applicable).

†The hydromagnesite content, calculated by TG.

‡The magnesite content, calculated from the CO_2 loss by TG.

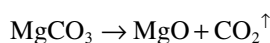
§The calcite content, calculated from the CO_2 loss by TG.

¶The insoluble residue after warm HCl (1:3).

||The soluble fraction = 100 – (insoluble residue + calcium carbonates + magnesium carbonates).

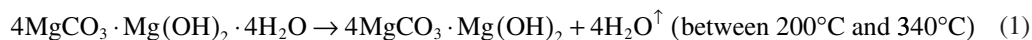
The most significant differences between the thermograms were detected in the range 200–650°C. In this temperature range, the losses vary from 1.45% (AM30) to 5.06% (AM23), perhaps due to the loss of binding structure water (dehydroxylation), and indicative of the presence of hydraulic compounds (e.g., calcium silicate hydrates, aluminium silicate hydrates: Elsen *et al.* 2010; Silva *et al.* 2011), which might justify the high values for AM28 (3.56%), AM33 (3.66%), AM34a (4.10%) and AM34b (3.80%), the samples that include ceramic fragments in their composition. In addition, also in that range of temperatures may occur dehydroxylation of clay minerals (Moropoulou *et al.* 1995a), the presence of which was identified by XRD; namely, kaolinite in AM23 (5.06%) and AM36 (3.07%), kaolinite and sepiolite in AM35 (2.25%) and chlorite in AM27 (4.72%).

The weight loss between 450°C and 550°C varies from 0.59% (AM9B) to 2.17% (AM29). In several studies about historical mortars, this range is attributed to decarbonation of magnesite, according to the equation

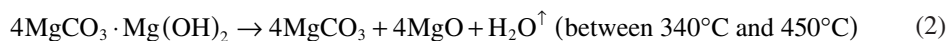


(Bruni *et al.* 1998; Paama *et al.* 1998; Adriano and Silva 2006a,b). Therefore, the low MgCO₃ contents (maximum 3.98%) are essentially compatible with a calcitic limestone with some magnesium carbonates (Table 3, 'MgCO₃ content') and this amount of magnesite would hardly be detected by XRD. Moreover, the results obtained in the TGA/DTA corroborate the XRD related to the non-identification of dolomite (losses between 520°C and 600°C).

A weight loss between 300°C and 400°C was detected in AM23 and AM27, which may be associated with the decomposition of hydromagnesite



and brucite



according to the above reactions (Bruni *et al.* 1998; Adriano and Silva 2006a).

The ratio between the weight loss due to the decomposition of carbonates (>650°C) and the weight loss attributed to hydraulic water (200–650°C) can express the hydraulic nature of the global fraction (Table 3, 'CO₂/H₂O') (Bakolas *et al.* 1998). Samples with high amounts of water bound to hydraulic compounds and, proportionally, small quantities of CO₂ are considered hydraulic (Elsen *et al.* 2010), as seen in AM28 (2.82), AM33 (3.89), AM34a (2.42) and AM34b (3.14), which includes the above-mentioned ceramic additives in its composition. Within this set of samples, AM34a should be noted, because it has a higher hydraulicity factor and corresponds to the sample that presents large ceramic fragments.

In the case of samples AM36, AM32 and AM23, which also present low hydraulicity factors, the results may be due to the low amount of binder and the presence of other products that are difficult to recognize and that present weight losses between 200°C and 650°C.

The remaining samples, in which the CO₂/H₂O ratio has reduced values, may include other compounds in their composition that also confer hydraulic properties, such as clay minerals (added to the carbonate rock at the calcination moment) or use carbonates with clays (marly limestone) or the accidental addition of residual earth; the value for AM9B may also be due to the reduced amount of binder (carbonate content, also confirmed by X-ray analyses). Rather, AM29

and AM30 have a higher $\text{CO}_2/\text{H}_2\text{O}$ ratio, corresponding to the samples with a lower hydraulicity factor, which relates to the DTG profile indicative of a composition rich in calcite. AM35 shows the higher $\text{CO}_2/\text{H}_2\text{O}$ ratio and it is the sample with a higher content of calcite, although the presence of clay minerals was detected by XRD.

In the DTA curve, an endothermic peak at 573°C was detected, without weight loss associated with TGA, which corresponds to the quartz transition phase $\alpha \rightarrow \beta$ (Newton and Sharp 1987; Moropoulou *et al.* 1995a; Montoya *et al.* 2003; Pires and Cruz 2007).

The similarities between the thermograms of AM29 and AM30 are evident, and may be related to the fact that these samples come from the same architectural complex—the public bath building—though from different structures (the wall masonry of the tank and an inside wall of the public bath building compartment, respectively), and have the same function, advancing with the possibility of being contemporary; that is, fit in the same construction phase.

The weight loss attributed to the chemically bound water of hydraulic compounds (200–650°C, excluding the magnesite and hydromagnesite contents, if applicable) and the soluble fraction could express the hydraulic nature of the global fraction (see Table 3, ‘Soluble fraction’). Their relation is expressed in Figure 6 and an acceptable linear correlation was obtained. That is, in most of the samples, the loss of water detected by thermal analysis in that temperature range corresponds, mostly, to the compounds that constitute the soluble fraction calculated by the Jedrzejewska method (1960); note that the soluble fraction = 100 – (insoluble residue + calcium carbonates + magnesium carbonates). So this soluble fraction excludes

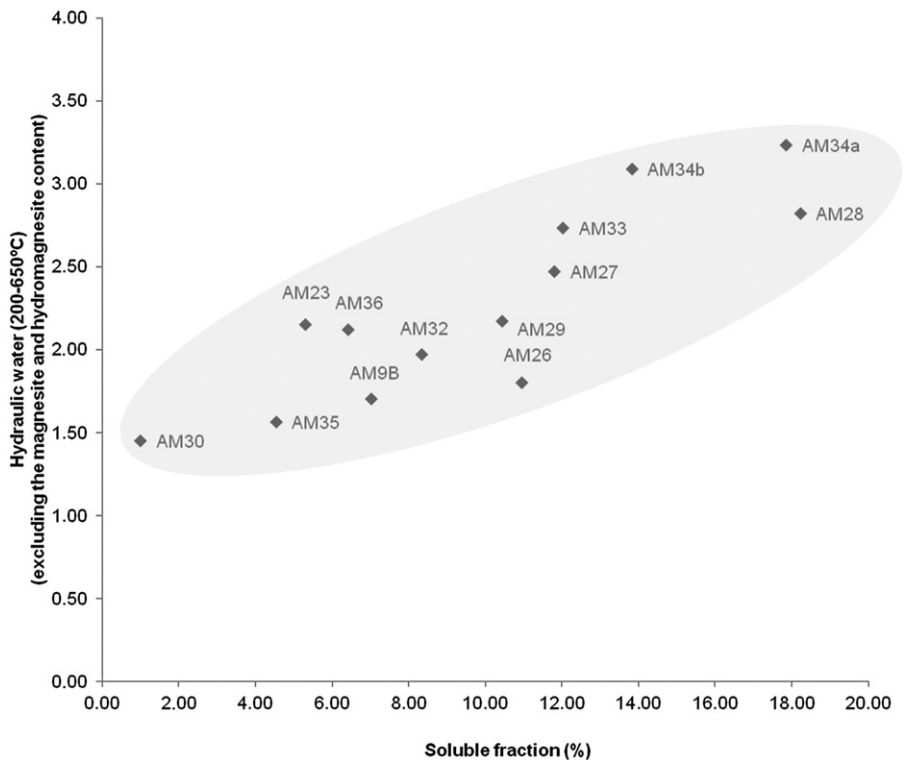


Figure 6 The soluble fraction versus the percentage weight loss between 200 and 650°C (excluding the eventual presence of magnesite and hydromagnesite), on the global fraction of the samples analysed by TGA/DTA.

the insoluble residue and the carbonates, retaining the contribution of eventual organic materials, soluble salts and hydraulic compounds, namely pozzolanic reaction products and clay materials.

Scanning electron microscopy with an energy-dispersive X-ray spectroscopy

With respect to *Ammaia* mortars, the polished surfaces of AM23, AM32, AM28 and AM34b, the two latter with crushed ceramic fragments, were analysed by SEM–EDS. Most of the samples have a compact microstructure, where it is possible to visualize the different constituent phases (the binder, lime lumps, the different aggregates and crushed ceramic fragments) well embedded in the binder matrix. Concerning the carbonate aggregates, SEM–EDS also did not reveal the presence of these particles. In sample AM23, a masonry mortar from the West Tower, possibly from a period after the Roman occupation (Table 1), many aggregates were detected, mostly fine-grained, which are related through the ratio 1:4 (soluble fraction:insoluble residue, Fig. 2) and the particle size distribution curve. In the matrix binder, the calcium to magnesium proportion correlates with the composition of a dolomitic lime: a Ca/Mg atomic ratio of 1.15 (Figs 7 (a) and 7 (b)). Furthermore, in this sample, some areas of the binder matrix present higher amounts of calcium, while others present higher amounts of magnesium, which is consistent with the presence of calcite and magnesite that are produced during the thermal decomposition of dolomite during lime production (Figs 7 (c) and 7 (d)). In the elemental maps, calcium and magnesium are in opposition to silicon, the main constituent of the silicate aggregates. In some areas of the binder matrix, the preferential association of aluminium with silicon was detected, possibly because of the presence of kaolinite, identified in the XRD. The lime lumps, considered as the closest indicator of the lime used at the moment of mortar preparation, are composed of magnesium and calcium in amounts that approximate the composition of a dolomitic limestone: Ca/Mg = 1.28.

In AM32, the association of magnesium, aluminium and silicon that was detected in the binder matrix, forming aluminium and magnesium silicates (Figs 7 (e) and 7 (f)), points to new compounds produced due to pozzolanic reactions. Calcium concentrates around the aggregates and fills the gaps (in the form of recrystallization of the calcite) (Figs 7 (g) and 7 (h)). As opposed to AM23, in AM32 the amount of calcium is higher than the magnesium, both in the recrystallization of the calcite (Ca/Mg = 26.3) and in the lime lumps (Ca/Mg = 18.05), and the composition is not compatible with that of a dolomitic limestone from the region (Figs 7 (i) and 7 (j), and see Fig. 1).

In the matrix binder of samples AM28 and AM34b, magnesium is dissociated from calcium and is in proportion to the aluminium and silicon, forming the above-mentioned magnesium aluminium silicate. Also, the areas adjacent to the ceramic fragments are enriched in these compounds, while calcium fills the gaps (Figs 7 (k) and 7 (l)). As in AM32, in the lime lumps of those samples, the calcium content predominates over the magnesium content (AM28, Ca/Mg = 5.34; AM34b, Ca/Mg = 8.39).

As for aggregates, in the general range of the analysed samples, the results obtained by SEM–EDS corroborate the XRD and the observations by stereozoom microscope, and particles with a strong predominance of silicon are identified—quartz, and others formed from silicon, aluminium and potassium (potassium feldspars) or sodium (sodium feldspar); and mica was identified from the association of silicon, aluminium, potassium. As has already been demonstrated in previous tests, the angular shape of the aggregates was confirmed.

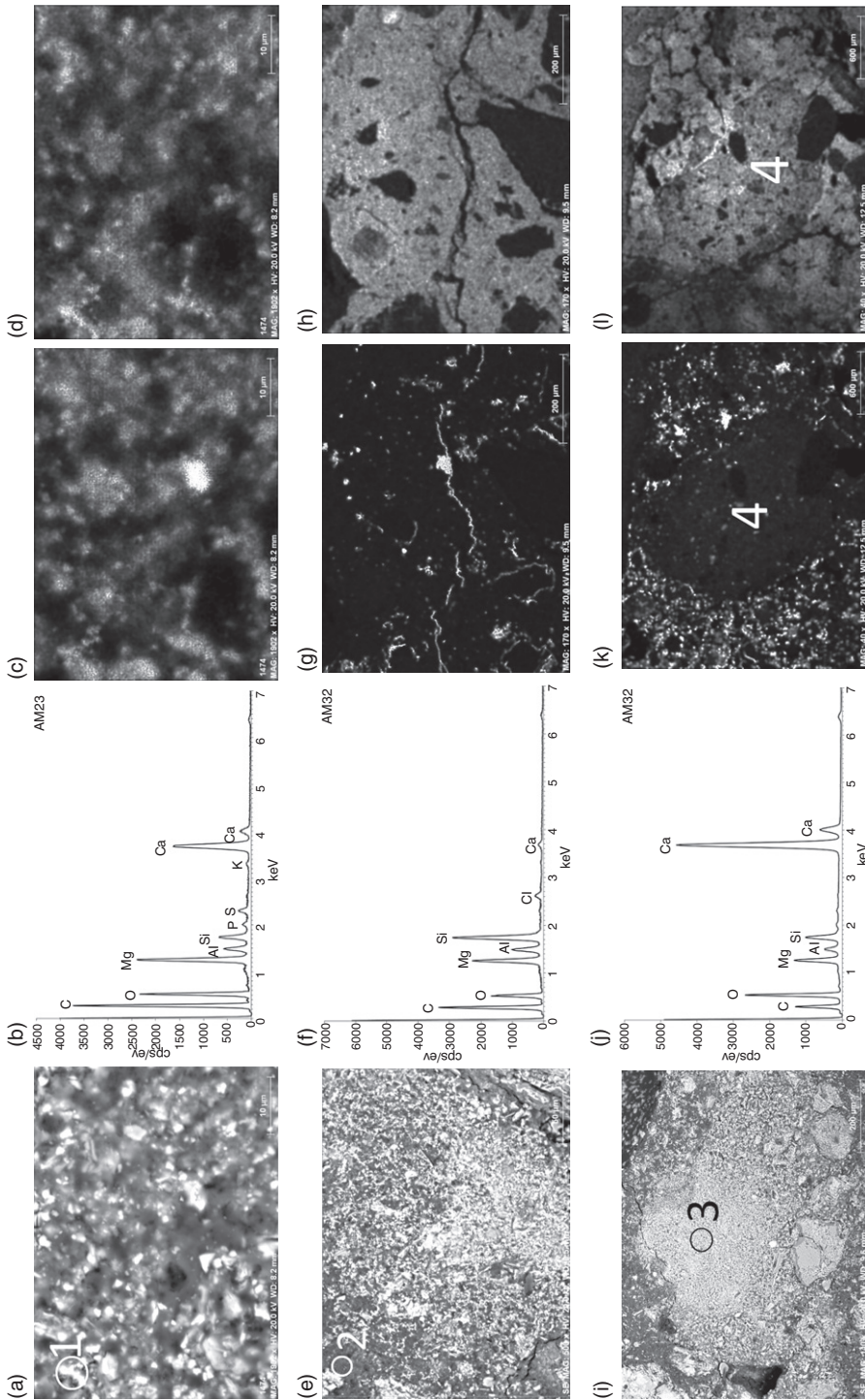


Figure 7 Sample AM23: (a) the general aspect of the binder and aggregates microstructure; (b) the corresponding EDS spectrum resulting from the punctual chemical analysis located on the image as '1'; binder; and distribution elemental maps of (c) calcium and (d) magnesium. Sample AM32: (e) the general aspect of the binder microstructure, with the silicates of aluminium and magnesium; (f) the corresponding EDS spectrum resulting from the punctual chemical analysis located on the image as '2'; distribution elemental maps of (g) calcium and (h) magnesium; (i) the general aspect of the AM32 lime lump microstructure; and (j) the corresponding EDS spectrum resulting from the punctual chemical analysis located on the image (i) as '3'. Sample AM28: distribution elemental maps of (k) calcium and (l) magnesium; ceramic fragment marked as '4'.

In samples AM28 and AM34, ceramic fragments were identified, composed of aluminium, magnesium, iron and well-defined particles of potassium, sodium, calcium (in small amount), silicon and titanium (residual).

General considerations

Apart from their locations and their function in the architectural structure, the characterization methodology allowed the following classification of the mortars, based on their composition (Table 4):

I. Mortars composed of a soil/clayish matrix (i.e., may include residual amounts of calcite) without additives: AM24.

II. Mortars whose binder is mostly calcite, in which magnesium carbonates, additives (ceramic fragments) or lime lumps were not identified—these are compatible with the burning of a calcitic limestone: AM29 and AM30.

Table 4 *A classification of the mortars on the basis of their composition*

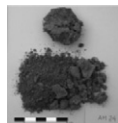
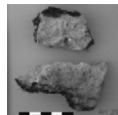
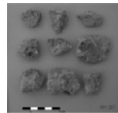
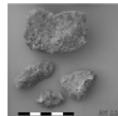
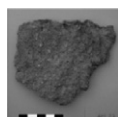
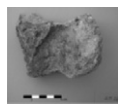
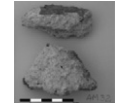
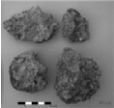
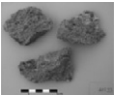
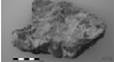
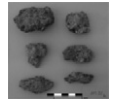
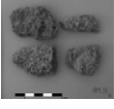

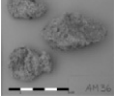
<i>Group</i>	<i>Binder composition</i>	<i>Lime lumps</i>	<i>Additives</i>	<i>Samples</i>	
I	Soil/clayish matrix (may include residual amounts of calcite)	–	–	AM24	
II	Calcite (magnesium carbonates were not identified); compatible with the burning of a calcitic limestone	–	–	AM29	
		–	–	AM30	
III	Calcite (with probable presence of magnesium carbonates—magnesite and hydromagnesite in greater amount, >2%); not compatible with the burning of a calcitic limestone	√	–	AM23	
		√	–	AM27	
IV	Calcite (the presence of magnesium carbonates in small amounts, <2%, was probable); compatible with the burning of a calcitic limestone	√	–	AM26	
		–	–	AM32	

Table 4 (Continued)

Group	Binder composition	Lime lumps	Additives	Samples	
V	Calcite (the presence of magnesium carbonates in small amounts, <2%, was probable); compatible with the burning of a calcitic limestone	√	√	AM28	
		–	√	AM33	
		√	√	AM34a,b	
		–	√*	AM31A	
		–	√*	AM31B	
		–	√*	AM35	
		–	√*	AM36	

Legend: √, detected; –, not detected; *, possible contamination.

III. Mortars whose binder is mostly calcite, in which the presence of magnesium carbonates—magnesite and hydromagnesite in greater amount (>2%)—is probable but additives were not identified—these are not compatible with the burning of a calcitic limestone: AM23 and AM27.

IV. Mortars whose binder is mostly calcite, in which magnesium carbonates were identified in small amounts (<2%) and not as visible additives—these are compatible with the burning of a calcitic limestone: AM26 and AM32.

V. Mortars whose binder is mostly calcite, in which small amounts of magnesium carbonates and additives (ceramic fragments) were identified—these are compatible with the burning of a calcitic limestone: AM28, AM33, AM34a and AM34b. Samples AM31A, AM31B, AM35 and AM36, in which additives were identified in residual amounts, may also be included within this group.

On the basis not only of the visual observations and optical microscopy, but also the XRD results, sample AM24 is very different from the others due to its strong brown colour. The main constituent of this sample is clay (without any significant addition of calcite in the binder composition) and it presents weak cohesion. This sample comes from archaeological structures

dated to the early period of the founding of the town (first century BC) and these findings confirm the assumptions of the archaeology team, that AM24 is an example of the first mortars used at the beginning of the Roman settlement.

Through the TGA/DTA, in the samples from group III (AM23, West Tower; and AM27, *peristylum*) weight losses in the temperature ranges 300–400°C and 450–550°C were identified, which, according to the literature (Moropoulou *et al.* 1995a; Bruni *et al.* 1998; Adriano and Silva 2006a,b), are attributed to the decomposition of hydromagnesite and magnesite, respectively, with higher contents than in the remaining samples (hydromagnesite—AM23, 4.31%; AM27, 5.55%; magnesite—AM23, 3.98%; AM27, 2.26%; calcitic binder—AM23, 9.37%; AM27, 16.72%). For AM23, lime lumps were also analysed by SEM–EDS, and are considered as the closest indicator of the lime used in the preparation of the mortar, resulting in a Ca/Mg ratio that can be correlated with the composition of a dolomitic limestone. In these samples, the non-detection of magnesium carbonates by XRD could possibly be due to the reduced amount of binder present in them—thus confirming the assumptions of the archaeology team, that AM23 and AM27 probably do not fit into the Roman period, and that the lime used as binder may come from local outcrops in the vicinity of the city, namely the dolomitic limestones of Escusa.

The binders of the mortars from the other groups are mainly constituted of calcite, especially the mortars from group II—AM29 and AM30 (both from the public bath building), in which, according to XRD and TGA/DTA, magnesium carbonates were not identified. These samples come from structures identified during the excavation that began in 1996, which fit into the Roman period.

On the samples from group IV (AM26, *macellum*; and AM32, the *podium* of the temple), the magnesium carbonate content determined by TGA/DTA is extremely reduced. SEM–EDS analysis of sample AM32 shows that the amount of calcium prevails over the magnesium, suggesting therefore that the composition of the binders is closer to that of limestone, rather than the local dolomitic limestones in the vicinity.

Even with regard to the analysis of the binders, a similar situation to that noted previously was identified from the group V samples, which come from the render of the inner part of the tank (AM28, public bath building) and the preparation of the floor of the *podium* of the temple (AM33, AM34a and AM34b), both buildings attributed to the period of Roman occupation.

Thus, there are also variations in the composition of the binders of the mortars, with implications for determination of the provenance of the limestone used in the lime preparation, which may be local (AM23 and AM27) or may come from another region. If the latter case pertains, it is assumed that the raw materials were carefully selected and that the Roman builders did not recognize the necessary quality of the local dolomitic limestone materials. In addition, there could have been preferential sites for the exploitation of the rocks for the lime production and, consequently, established commercial routes. On the other hand, it appears that this compositional variation may be related to different historical contexts: the composition of the binders of the mortars that fall into the Roman period is not correlated with the limestone of the region, while the binders of the mortars subsequent to the Roman occupation may have a local provenance.

In this study is also noted the preferential association among magnesium, aluminium and silicon, dispersed by the binder matrix and detected by SEM–EDS, both in samples where ceramic fragments are visible (e.g., AM28 and AM34b) and those in which these were not identified (e.g., AM32); those silicates of magnesium and aluminium were not detected by XRD, possibly because they are amorphous. The origin of these compounds was not conclusive at this stage of the study, however, they may be related to:

- neof ormation products, probably with hydraulic characteristics, resulting from the pozzolanic reactions (particularly in the samples with ceramic fragments); or
- the presence of clay minerals or amorphous materials with similar characteristics, resulting from a deliberate addition at the moment leading up to the calcination of the limestone, in order to optimize the properties of the mortars, according to the objectives (e.g., a mortar with hydraulic properties is more resistant than one made of aerial lime) (Elsen *et al.* 2010).

Even in the mortar of group V, crushed ceramic fragments were identified and used like additives, with different orange/red hues and grain sizes. The presence of this additive is well known for Roman mortars, and has also already been detected in several studies of Roman mortars in Portugal (Ricardo *et al.* 2005; Silva *et al.* 2006a,b; Velosa *et al.* 2007; Borsoi *et al.* 2010). This practice is recommended in book VII, chapter IV of Vitruvius for the improvement of the performance of the lime-based mortars in moist environments, which occurs in AM28, the render on which were placed the marble slabs that covered the interior walls of the tank. The use of these additives gives hydraulic properties to the mortars, allowing them to harden in moist environments, become waterproof and increase their durability (Elsen *et al.* 2010). On the other hand, Vitruvius also recommends the application of crushed ceramic fragments in the mortar used in the *nucleus*, the hard and compact layer that would become the render of a pavement surface, as seen in mortars AM33 and AM34a,b, collected from the floor of the *podium* of the temple (Vitruvius 2006, book VII, chapter I), also making them more resistant and waterproof. In most of the analysed samples, the aggregates are siliceous: quartz (crystal and milky), feldspars and micas, with a possible provenance from the local granites, either crushed on site or from river sediments, but near the outcrops, because the angular shape is predominant, indicating transportation of the aggregates over a short distance.

CONCLUSIONS

The methodology for the characterization of the *Ammaia* mortars used in this study consists of the application of various physical and chemical techniques that complement each other. The results of this approach are a series of consistent data that have allowed us to address specific goals.

Mortar constituents, provenance of raw materials, historical context

Different groups of mortars were identified on the basis of their composition, distinguishing sample AM24, which has no significant addition of carbonate binder, and that comes from the architectural structures considered to represent the beginning of Roman occupation of the settlement. The remaining samples, those whose binder composition is not correlated with the dolomitic limestone of the region, were distinguished and are likely to be from the Roman period. On the other hand, samples AM23 (West Tower) and AM27 (*peristylum*) can be correlated with the use of dolomitic lime from local quarries (Fig. 4), which are likely to be from a period later than the Roman occupation (Islamic rebuilding or a farm from the 17th century). Thus, a relationship between the composition and its historical context was established, confirming the assumptions defined by the archaeology team.

Technical production

One possible option was not to use local raw materials in the preparation of lime, and to make deliberate use of crushed pottery fragments (hydraulic compounds) in mortars that would be in

contact with moist environments. These facts are characteristic of the knowledge that Roman civilization (or constructors) had on construction technologies. Similar to other studies on Roman mortars, in this work it is evident that this civilization had deep knowledge concerning the selection and combination of raw materials to obtain mortars with specific properties, which was based on visual observation and empirical knowledge, in order to comply with the defined construction objectives and respect the construction treatises at the time.

Variation of the composition according to function

The characterization of the mortars allowed their distinction by function in the architectural structure; for example, the composition of masonry mortars that differ from the renders applied as a coating inside the tank and the preparation of the temple floor; and in the latter, the presence of crushed pottery fragments visible, with variable grain size, a practice recommended by Vitruvius in *De architectura*. The variation of the composition of the mortars was more evident in terms of its role in the architectural structure (masonry versus render) and its historical context than in terms of the social importance of the building under study.

Conservation and restoration

The non-functional joints due to a lack of fill mortar, or to insufficient mortar to bond the stone blocks, the existence of joints filled up to the face of the blocks and the different degrees of cohesion of the mortar are some factors that influence the approach to the conservation and restoration of the archaeological structures, which is far from simple and consensual. The importance of the mortar in this process is crucial, and it is indispensable to consider the need to consolidate the pre-existing mortar with compatible materials. Consequently, in the reported characterization of the binders and aggregates, the determination of the binder:aggregates ratio constitutes a fundamental support in the development of a working concept for the conservation of the archaeological structures, based on compatibility between the pre-existing materials and the restoration mortar.

ACKNOWLEDGEMENTS

The authors wish to acknowledge the Fundação para a Ciência e Tecnologia for financial support (Ammaia Project—PTDC/HIS-ARQ/103227/2008 and GODESS Project—PTDC/HIS-ARQ/108758/2008). The authors also wish to thank Sara Valadas, Luís Dias and Nuno Carriço (HERCULES Laboratory, University of Évora), Sandra Velez (Geosciences Department, University of Évora) and Joaquim Carvalho, Dulce Osório, Valentina Castro (CIDEHUS, University of Évora).

REFERENCES

- Adriano, P., and Santos Silva, A., 2006a, *Caracterização de argamassas antigas da Igreja de Santa Maria de Évora—Sé Catedral de Évora*, Relatório 59/06 NMM, LNEC, Lisboa.
- Adriano, P., and Santos Silva, A., 2006b, *Caracterização de argamassas do período romano e árabe da Vila de Mértola*, Relatório 200/06 NMM, LNEC, Lisboa.
- Bakolas, A., Biscontin, G., Moropoulou, A., and Zendri, E., 1998, Characterization of structural Byzantine mortars by thermogravimetric analysis, *Thermochimica Acta*, **321**, 151–60.

- Borsoi, G., Santos Silva, A., Menezes, P., Candeias, A., and Mirão, J., 2010, Chemical, mineralogical and microstructural characterization of historical mortars from the Roman villa of Pisões, Beja, Portugal, in *2nd Historic Mortars Conference HMC2010 and RILEM TC 203-RHM Final Workshop, 22–24 September 2010, Prague, Czech Republic* (eds. J. Válek, C. Groot and J. J. Hughes), 43–54.
- Bruni, S., Cariati, F., Fermo, P., Pozzi, A., and Toniolo, L., 1998, Characterization of magnesian mortars coming from northern Italy, *Thermochimica Acta*, **321**, 161–5.
- Callebaut, K., Elsen, J., Van Balen, K., and Viaene, W., 2001, Nineteenth century hydraulic restoration mortars in the Saint Michael's Church (Leuven, Belgium)—natural hydraulic lime or cement? *Cement and Concrete Research*, **31**(3), 397–403.
- Delgado Rodrigues, J., and Grossi, A., 2007, Indicators and ratings for the compatibility assessment of conservation actions, *Journal of Cultural Heritage*, **8**, 32–43.
- Duarte, I. M. R., Ladeira, F. L., and Gomes, C. F., 2000, Características geológico-geotécnicas do solo residual do granito de Marvão (Portalegre), in *Actas do VII Congresso Nacional de Geotecnica*, vol. 1, 151–60, Porto.
- Elsen, J., Balen, K. V., and Mertens, G., 2010, Hydraulicity in historic lime mortars: a review, in *2nd Historic Mortars Conference HMC2010 and RILEM TC 203-RHM Final Workshop, 22–24 September 2010, Prague, Czech Republic* (eds. J. Válek, C. Groot and J. J. Hughes) 29–145.
- ICOMOS–ISCS, 2008, *Illustrated glossary on stone deterioration patterns*, Monuments and Sites XV, ICOMOS, Paris.
- Jedrzejska, H., 1960, Old mortars in Poland: a new method of investigation, *Studies in Conservation*, **5**, 132–8.
- Montoya, C., Lanas, J., Arandigoyen, M., Navarro, I., García Casado, P. J., and Alvarez, J. I., 2003, Study of ancient dolomitic mortars of the church of Santa María de Zamarce in Navarra (Spain): comparison with simulated standards, *Thermochimica Acta*, **398**, 107–22.
- Moropoulou, A., Bakolas, A., and Bisbikou, K., 1995a, Characterization of ancient, Byzantine and later historic mortars by thermal and X-ray diffraction techniques, *Thermochimica Acta*, **269/270**, 779–95.
- Moropoulou, A., Bakolas, A., and Bisbikou, K., 1995b, Thermal analysis as a method of characterizing ancient ceramic technologies, *Thermochimica Acta*, **2570**, 743–53.
- Munsell Color, 1992, *Munsell Soil Color Charts*, revised edn, Macbeth, Division of Kollmorgen Instruments Corp., Newburgh, New York.
- Newton, R. G., and Sharp, J. H., 1987, An investigation of the chemical constituents of some Renaissance plasters, *Studies in Conservation*, **32**, 163–75.
- Paama, L., Pitkänen, I., Rönkkömäki, H., and Perämäki, P., 1998, Thermal and infrared spectroscopic characterization of historical mortars, *Thermochimica Acta*, **320**, 127–33.
- Perdigão, J. C., and Fernandes, A. P., 1976, *Geological map of Portugal, 29-C Marvão, scale 1/50000*, Geological Survey of Portugal.
- Pires, J., and Cruz, A. J., 2007, Techniques of thermal analysis applied to the study of cultural heritage, *Journal of Thermal Analysis and Calorimetry*, **87**(2), 411–15.
- Ricardo, J. M., and Santos Silva, A., 2005, *Caracterização de argamassas romanas*, Relatório 28/05 NMM, LNEC, Lisboa.
- Schiavon, N., and Mazzocchin, G. A., 2009, The provenance of sand in mortars from Roman villas in NE Italy: a chemical–mineralogical approach, *The Open Mineralogical Journal*, **3**, 32–9.
- Silva, A. S., Paiva, M., Ricardo, J., Salta, M., Monteiro, A. M., and Candeias, A. E., 2006a, Characterisation of Roman mortars from the archeological site of Tróia (Portugal), *Materials Science Forum*, **514–16**, 1643–7; <http://cathedral.lnec.pt/publicacoes/a5.pdf>
- Silva, A. S., Cruz, T., Paiva, M. J., Candeias, A., Adriano, P., Schiavon, N., and Mirão, J. A. P., 2011, Mineralogical and chemical characterization of historical mortars from military fortifications in Lisbon harbour (Portugal), *Environment Earth Science*, **63**, 1641–50.
- Silva, A. S., Ricardo, J. M., Salta, M., Adriano, P., Mirão, J., Candeias, A. E., and Macias, A., 2006b, Characterization of Roman mortars from the historical town of Mértola, in *Heritage, weathering and conservation* (eds. R. Fort, M. Alvarez De Buergo, M. Gomez-Heras and C. Vasquez-Calvo), vol. I, 85–90, Taylor & Francis, London.
- Veiga, M. R., Aguiar, J., Silva, A. S., and Carvalho, F., 2004, *Conservação e renovação de revestimentos de paredes de edifícios antigos*, LNEC, Lisboa.
- Velosa, A. L., Coroado, J., Veiga, M. R., and Rocha, F., 2007, Characterization of Roman mortars from Conímbriga with respect to their repair, *Materials Characterization*, **58**, 1208–16.
- Vermeulen, F., and Taelman, D., 2010, From cityscape to landscape in Roman Lusitania: the *municipium* of *Amaia*, in *Changing landscapes—the impact of Roman towns in the Western Mediterranean, Proceedings of the International Colloquium, Castelo de Vide—Marvão 15th–17th May 2008* (eds. C. Corsi and F. Vermeulen), 311–24.
- Vitrúvio, 2006, *Tratado de arquitectura* (tradução do latim, introdução e notas por M. Justino Maciel), IST PRESS, Lisboa.